

Title No. S118-132

A Shear Hinge Model for Analysis of Reinforced Concrete Beams

by Amir Reza Tabkhi Wayghan and Vahid Sadeghian

The lumped plasticity method is an efficient analytical approach to assess the system-level performance of reinforced concrete (RC) structures. Through this analysis approach, the nonlinearity effects are calculated using plastic hinges located in critical parts of the structure. Because of the complexity associated with shear-related mechanisms in RC members, the number of shear hinge models developed in the literature are limited. This paper presents a comprehensive shear hinge model for RC beams capable of capturing advanced mechanisms such as interactions between shear force and bending moment, effects of nonlinear stress and strain distributions through the section, and compression softening effect in concrete. The model provides closed-form equations for five key points on the shear force-shear deformation response by satisfying the compatibility, equilibrium, and constitutive relationships. By comparing the performance of the model against test results, other analysis methods, and design codes at the component and system level, the effectiveness of the model in capturing the shear behavior is demonstrated.

Keywords: lumped plasticity; nonlinear analysis; reinforced concrete (RC) beams; shear behavior.

INTRODUCTION

Despite significant research over the last few decades, computing the shear behavior of reinforced concrete (RC) structures has still remained a challenging task. The shear response is not only dependent on complex material mechanisms, but can also be highly influenced by flexural and axial forces in a section. Besides, shear failure is inherently a brittle type of failure that could occur almost without warning, making it extremely dangerous. Catastrophic shear failures in recent years (for example, shear failure of Sleipner A offshore platform in 1991¹ and failure of the De la Concorde overpass bridge in 2006²) have forced engineers and researchers to develop analytical models capable of accurately predicting the shear response in RC structures.

Detailed finite element (FE) modeling with powerful two-dimensional (2-D) and three-dimensional (3-D) elements is perhaps the most accurate method for analyzing structures. However, because of the high computational demand and modeling effort, application of this method is mostly limited to analysis of RC structures at the component level (beams, columns, and so on). For system-level analysis of RC structures, engineers typically use frame-type analysis methods because of their computational efficiency and simplicity in modeling. Nonlinearity effects in frame-type analysis are taken into account based on either a distributed plasticity method or a lumped plasticity approach. The distributed plasticity approach (also known as fiber-based approach) calculates the nonlinear stresses and strains over

the entire length of members typically based on the assumption that plane sections remain plane, while the lumped plasticity approach assumes that nonlinearity is concentrated at predefined critical locations (that is, plastic hinges) and that the remaining part of members have a linear elastic behavior. The majority of frame-type modeling methods are developed for analysis of RC structures under flexural loads and cannot accurately take into account the shear behavior. Considering the importance of system-level analysis in the performance assessment of RC structures, there is a great need for the development of computationally efficient frame-type modeling methods capable of capturing the shear behavior.

The lumped plasticity method is computationally more efficient than the distributed plasticity method, making it more suitable for the analysis of large structural systems or when large number of analyses are required. However, as mentioned previously, most plastic hinges are developed for computing the flexural response (for example, flexural plastic hinges by Bouchaboub and Samai³ and Simão et al.⁴), and the number of shear plastic hinges is limited due to the complexity of shear behavior. Pincheira et al.⁵ presented a lumped plastic model for concrete columns that accounted for shear and flexural responses separately. Neglecting the flexural-shear interaction effects influenced the accuracy of the model in predicting the shear behavior. Shirai et al.⁶ formulated a macro element that considered both flexural and shear effects. However, they neglected the strength reduction due to concrete cracking and assumed the crack orientation remains constant throughout the analysis. Elwood⁷ introduced a shear hinge model with a trilinear response that incorporated a shear failure surface to determine the peak strength. The model was capable of capturing the response of RC columns under shear and axial loads and could account for shear strength degradation. However, it neglected the interaction effects between shear and bending moment. LeBorgne and Ghannoum⁸ proposed a similar analytical model for RC columns that consisted of a zero-length shear spring placed in series with flexural elements. Although the model was capable of capturing nonlinearity effects and strength degradation due to shear, it required the calibration of strength and stiffness parameters prior to the analysis. Sae-Long et al.⁹ presented a nonlinear fiber frame element enhanced with a trilinear shear hinge model

ACI Structural Journal, V. 118, No. 6, November 2021.

MS No. S-2020-512.R1, doi: 10.14359/51733001, received May 25, 2021, and reviewed under Institute publication policies. Copyright © 2021, American Concrete Institute. All rights reserved, including the making of copies unless permission is obtained from the copyright proprietors. Pertinent discussion including author's closure, if any, will be published ten months from this journal's date if the discussion is received within four months of the paper's print publication.

for analysis of RC columns prone to shear or flexure-shear failure. Closed-form equations were proposed for the shear hinge model that considered strength degradation through a reduction factor calculated based on the curvature ductility of columns. In addition to the analytical models available in the research literature, ASCE/SEI-41¹⁰ recommends a generalized load-displacement backbone curve that can be used to define shear plastic hinges for RC members. The backbone curve is presented in a normalized form to generalize its application. Thus, it requires defining the shear strength and deformation at the yielding point by the user.

This paper presents a new lumped plasticity model for analysis of shear-critical RC beams developed based on the Modified Compression Field Theory (MCFT).¹¹ The MCFT is a smeared rotating crack model that treats stresses and strains in an average sense and allows cracks to gradually reorient as a result of change in loading or material behavior. Over the past 35 years, MCFT has been extensively verified against experimental tests, adapted to structural design codes, and implemented into various types of FE and sectional analysis software.¹² These efforts have shown the ability of MCFT for computing the response of RC structures, particularly under shear. This paper, for the first time, extends the application of MCFT to analysis of shear-critical

RC beams with and without shear reinforcement using the lumped plasticity approach.

RESEARCH SIGNIFICANCE

Compared with flexural hinge models, the number of shear hinge models available in the literature for analysis of shear-critical RC structures is limited. Most of the existing shear hinge models are unable to take into account the interactions between shear force and bending moment or consider advanced mechanisms in RC (for example, compression softening in concrete).

This paper addresses the limitations of existing models by presenting a comprehensive shear hinge model developed based on a rational theory capable of capturing nonlinear shear effects. The proposed model is expected to improve the system-level performance assessment of RC structures by accounting for shear deformations and shear failure modes.

MODEL DEVELOPMENT

The proposed lumped plasticity model estimates the shear force versus shear strain relationship by calculating five key points on the response: flexural cracking, shear cracking, yielding of shear reinforcement, ultimate shear strength, and shear failure. Figure 1 shows a schematic representation of the shear force-shear strain response used in the model, including the key points. A 2-D panel element is used to simulate the nonlinear shear behavior of the beam in a concentrated manner, as shown in Fig. 2. Unlike one-dimensional spring elements used in most existing plastic hinge models, using a 2-D panel element enables capturing interactions between axial, flexural, and shear forces. Closed-form equations (Eq. (1) to (9)) are developed based on MCFT to determine the shear force and shear strain values at the key points. These equations simplify the original formulation of MCFT, which is complicated and requires a trial-and-error procedure, making it suitable for lumped plasticity analysis. The formulation of MCFT used in the derivation of closed-form equations is shown in Fig. 2. The model considers the nonlinear distribution of various parameters, such as crack inclination (θ), shear strain (γ), and shear stress (v) through the section in an average sense. Using a large number of sectional analyses performed based on the full MCFT model on a wide range of shear-critical RC beams, the nonlinear

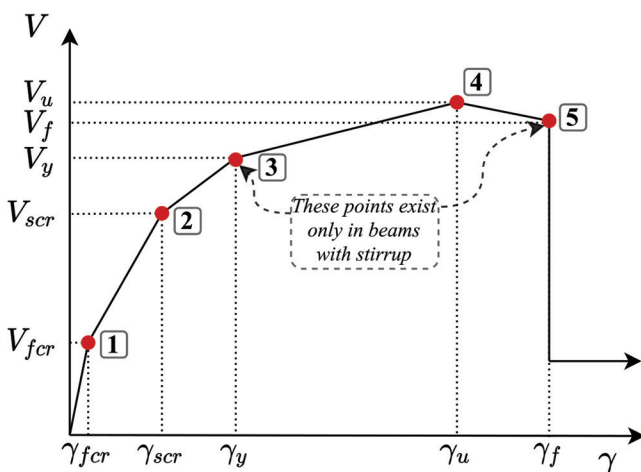


Fig. 1—Schematic shear force-shear strain response of proposed model.

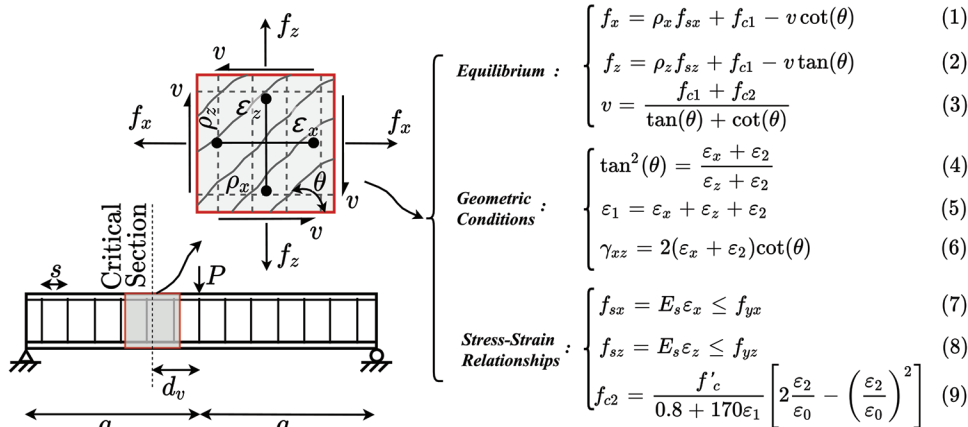
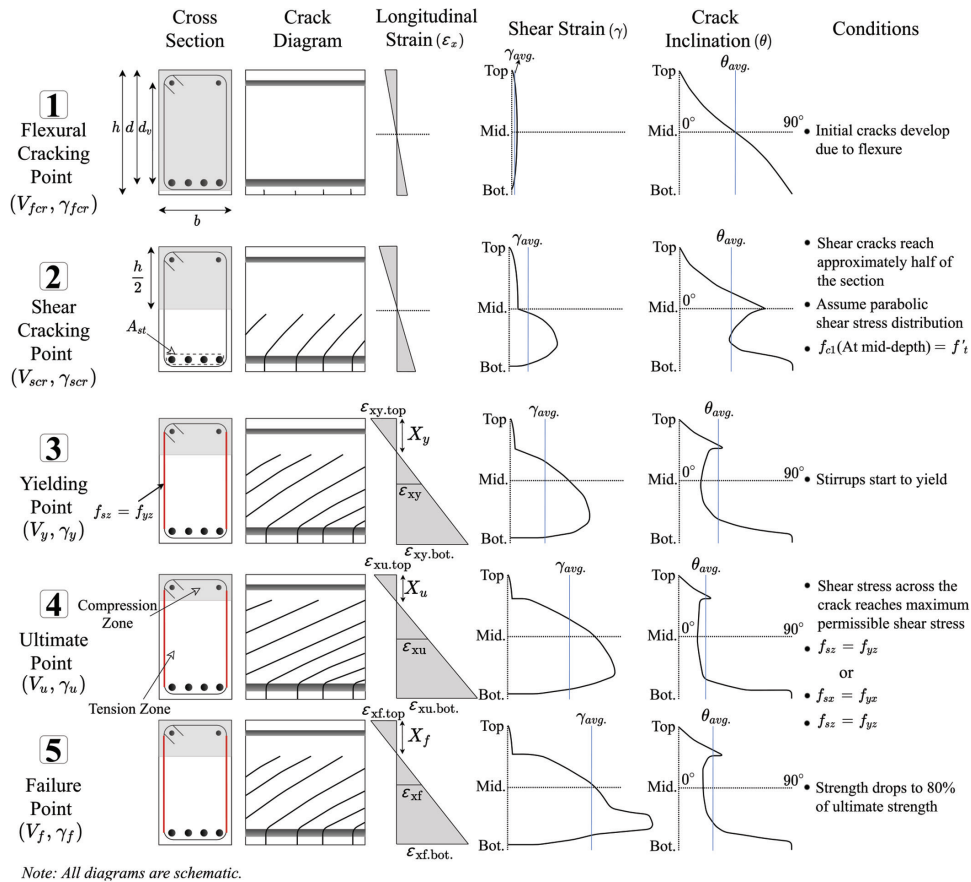


Fig. 2—Representing shear behavior of beam in concentrated manner with panel element formulated based on MCFT equations.



Note: All diagrams are schematic.

Fig. 3—Variations of longitudinal and shear strains and crack direction through section at five key points of response.

distribution of each parameter at different stages of the response is determined. The models are selected such that they cover a wide range of important parameters such as concrete compressive strength (from 20 to 100 MPa [2900 to 14,500 psi]), yield strength of reinforcing bars (from 300 to 600 MPa [43,500 to 87,000 psi]), beam height (from 200 to 2000 mm [7.87 to 78.74 in.]), cross-sectional dimension ratio (h/b) (from 0.8 to 8.0), and the transverse reinforcement ratio (ρ_z) between 0.00% and 2.25%. Simple equations are developed to approximate the nonlinear distribution with an average value for the entire 2-D panel representing the shear hinge in the beam. This approach makes it possible to develop a relatively simple model for lumped plasticity analysis that can capture nonlinearity effects with reasonable accuracy. The typical distribution of shear strain, longitudinal strain, and crack inclination along the beam height found from sectional analyses based on the full MCFT model are shown in Fig. 3. In the following, the development of closed-form equations for the key points of the response is discussed.

Ultimate point

The shear strength (V_u) is calculated based on the shear design provisions of the Canadian concrete design code, CSA A23.3,¹³ with some modifications. According to CSA A23.3, which is developed based on the MCFT model, the shear strength of a beam section can be expressed as

$$V_r = V_c + V_s = \beta \sqrt{f'_c} b d_v + \frac{A_{st} f_{yt} d_v}{s} \cot(\theta_u) \quad (10)$$

where V_c and V_s are the shear strength of concrete and transverse reinforcement; β is the contribution factor accounting for the strength of cracked concrete; and θ_u is the inclination of crack at the peak shear stress. In the CSA A23.3 procedure, θ_u is considered to be equal to $(29 + 7000\epsilon_x)$, where ϵ_x is the longitudinal strain at middepth of the member. However, Bentz et al.¹⁴ and Esfandiari and Adebahr¹⁵ showed that for beams with stirrups the crack direction at ultimate load depends not only on ϵ_x , but also on the ratio of the yielding stress in the shear reinforcement to the compressive strength of concrete $\rho_z \times f_{yt}/f'_c$. To perform a more thorough investigation, a wide range of RC beam sections with different ratios of $\rho_z \times f_{yt}/f'_c$ is analyzed in this study using Response-2000,¹⁶ which is a nonlinear sectional analysis software developed based on MCFT. The relationship between θ_u and ϵ_x calculated for different beams as well as the code predictions is shown in Fig. 4. It can be seen that because the influence of stresses in concrete and steel on θ_u is neglected, CSA A23.3 provides an upper bound for θ_u , which results in conservative shear strength values. Using data presented in Fig. 4, a more refined equation for θ_u is developed for beams containing shear reinforcement (refer to Eq. (11)).

For beams without shear reinforcement, Bentz et al.¹⁴ showed that θ_u is approximately equal to $(29 + 7000\epsilon_x) \cdot (0.88 + s_{ze}/2500)$, where s_{ze} is the crack spacing parameter estimated using equations in the Appendix. In this

study, using a parametric analytical study similar to that used for beams with stirrups, it is found that by relating θ_u to the square root of ε_x instead of ε_x , a more accurate equation for predicting θ_u can be obtained. This is shown in Fig. 5, where the predictions of the proposed equation are compared with the results of the full MCFT model reported by Bentz et al.¹⁴ The proposed equations for calculating θ_u for both cases of beams with and without stirrups are shown in Eq. (2). All k_i coefficients are described in the Appendix.

$$\theta_u = \begin{cases} (29 + 7000\varepsilon_x) \cdot (k_6) & \text{with stirrups} \\ \left[29 + (k_7)\sqrt{\varepsilon_x} \right] \cdot (k_6) \geq 29 & \text{without stirrups} \end{cases} \quad (11)$$

To find the shear strength in CSA A23.3, ε_x is calculated using the shear force (V_f) acting on the section. As the shear force increases, ε_x increases, resulting in a lower shear

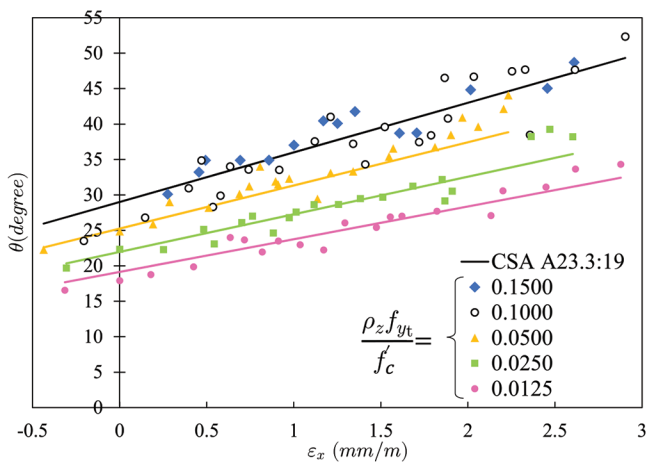


Fig. 4—Comparison of crack inclination θ predicted by Response-2000 and CSA A23.3 for various values of $\rho_z \times f_{yt} / f_c'$ in beams with stirrups.

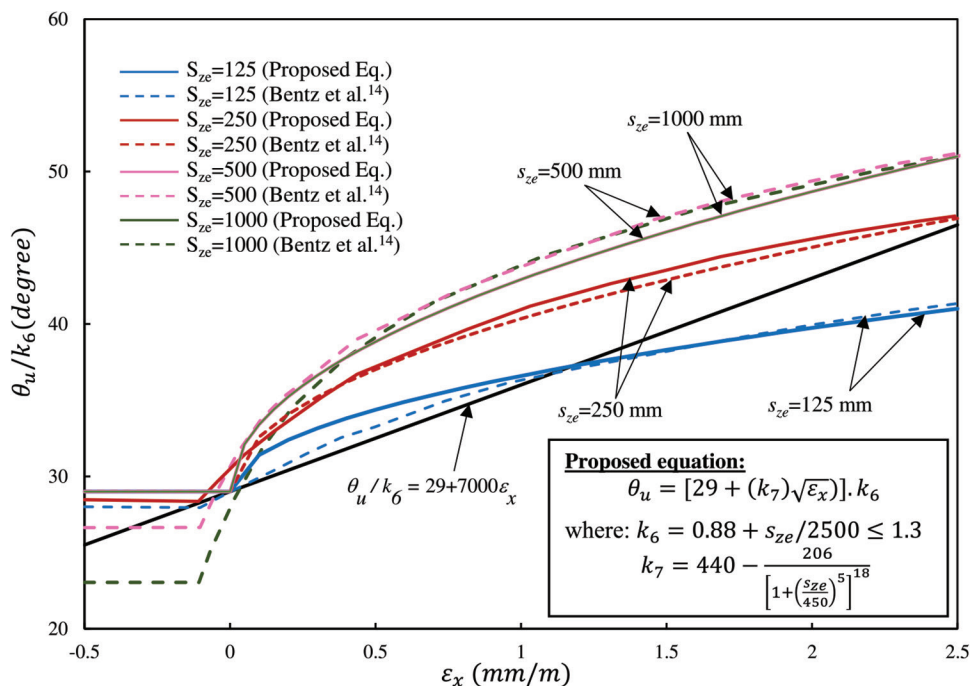


Fig. 5—Comparison of crack inclination (θ) predicted by full-MCFT method and proposed equation in beams without stirrups.

strength. The relationship between the applied shear force and the shear strength for a section is shown in Fig. 6. While this procedure works for designing a section with known sectional forces, it cannot be applied for an analysis case where sectional forces are not known prior to the analysis. In this study, by recognizing that the maximum applicable shear force on a section (V_u) occurs when the shear resistance becomes equal to the applied shear force ($V_r = V_f$) (refer to Fig. 6) and by estimating $\cot(\theta_u)$ as $(1.73 - 300\varepsilon_x)(\rho_z \times f_{yt}/f_c')^{0.23}$, a new equation is derived to express the shear strength solely in terms of cross-section dimensions and material properties of the beam

$$V_u = \frac{k_1 k_3 - k_4}{2k_1 k_4} + \sqrt{\left(\frac{k_1 k_3 - k_4}{2k_1 k_4} \right)^2 + \frac{k_2 + k_3}{k_1 k_4}} \quad (12)$$

In some cases where the flexural capacity of the beam is low, the longitudinal reinforcement may yield before beam reaches its ultimate shear capacity. When the transverse and longitudinal reinforcements both yield, there would not be additional capacity in the reinforcing bars to equilibrate the diagonal compression force in the concrete, resulting in a shear strength lower than that predicted by Eq. (12). For these cases, Esfandiari and Adebar¹⁵ proposed an equation to calculate the shear strength of RC beam sections

$$V_u = \sqrt{(\alpha k_{15})^2 + 2k_{15} A_s f_{yt}} - \alpha k_{15} \quad (13)$$

where α is the ratio of the bending moment to the shear force times the effective shear depth ($M/(V \times d_v)$). In this study, the minimum value of Eq. (12) and (13) is taken as the shear strength for the lumped plasticity analysis.

The ultimate shear strain (γ_u) is found from Eq. (6) of the original MCFT model multiplied by a factor accounting for the effective shear strain depth in beams (k_9), as the shear

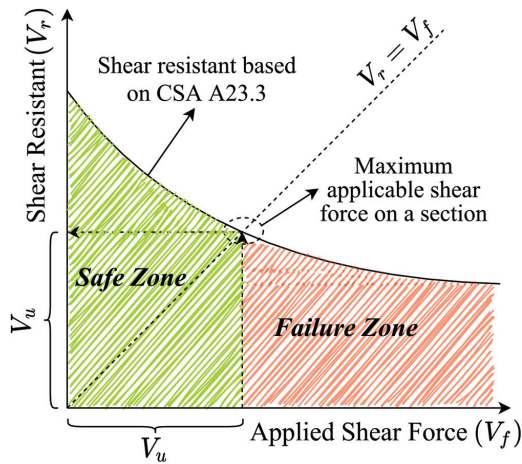


Fig. 6—Variation of shear strength with applied shear force according to CSA A23.3.

strain in the compression zone is almost equal to zero (refer to Fig. 3)

$$\gamma_u = 2(\epsilon_{xu} + \epsilon_{2u}) \cdot \cot(\theta_u) \cdot k_9 \quad (14)$$

where ϵ_{xu} and ϵ_{2u} are the longitudinal strain at middepth and average principal compressive strain of the section at the peak shear stress, respectively; and θ_u is the crack direction at the peak shear stress, which can be determined from Eq. (11). CSA A23.3¹³ approximates ϵ_{xu} to be equal to one-half of the strain in the flexural tensile reinforcement by assuming that the longitudinal strain at the top of the section is negligible. This is generally a conservative assumption that may be reasonable for calculating the shear strength, but it can result in inaccurate shear strain predictions. To obtain a more accurate estimation of ϵ_{xu} , the longitudinal strain at the top of the section needs to be considered, which requires estimating the height of the compression zone (X_u) (refer to Fig. 3). X_u can be calculated using Eq. (15) developed based on the equilibrium of the compression and tension forces in the section. According to Bentz and Collins,¹⁷ the tension force in the reinforcement is equal to $M_u/d_v + 0.5\cot(\theta_u)V_u$. In beams with stirrups, the typical range of θ_u varies between 20 and 35 degrees, while in beams without stirrups, θ_u is generally higher than 40 degrees. For simplicity, $0.5\cot\theta_u$ can be assumed to be equal to 1.0 and 0.0 for beams with and without stirrups, respectively. Additionally, the compression force in the concrete is determined to be $0.72f'_c b X_u$ from the equivalent rectangular stress block procedure.¹⁸ For beams without stirrups, however, the 0.72 factor is replaced with a term proportionally related to h and the square root of f'_c . Thus, X_u can be determined using Eq. (15). After determining X_u , ϵ_{xu} can be found from Eq. (16) by calculating k_1 and k_5 factors using equations provided in the Appendix.

$$X_u = \begin{cases} \frac{\min((\alpha + 1)V_u, A_{st} \cdot f_{yt})}{0.72 f'_c \cdot b} & \text{with stirrups} \\ \frac{\min(\alpha V_u, A_{st} \cdot f_{yt})}{\left[56(h \cdot \sqrt{f'_c})^{-0.7}\right] f'_c \cdot b} & \text{without stirrups} \end{cases} \quad (15)$$

$$\epsilon_{xu} = \left| \frac{k_1 V_u}{750} \cdot k_5 \right| \quad (16)$$

If imperial units are being used, the 56 in Eq. (15) should be replaced by 33.

The second parameter in Eq. (14) for determining γ_u is ϵ_{2u} . To calculate this parameter, first, the principal compressive stress in concrete (f_{c2u}) is determined from Eq. (3) of the original MCFT model. In this equation, the average principal tensile stress in concrete (f_{c1u}) is neglected, considering that concrete is heavily cracked at this stage of the response. Thus, f_{c2u} can be expressed as

$$f_{c2u} = v_u (\tan\theta_u + \cot\theta_u) \quad (17)$$

f_{c2u} can also be determined from Eq. (9) of the original MCFT model, which represents compressive stress-strain response of concrete based on the Hognestad model¹⁹ while including the compression softening effect. By equating Eq. (17) to Eq. (9) and using Mohr's circle of strains, the following equation can be found for ϵ_{2u}

$$\epsilon_{2u} = k_8 \cdot \epsilon_0 \quad (18)$$

where ϵ_0 is the strain corresponding to the compressive peak strength of concrete; and k_8 is a factor provided in the Appendix in terms of the concrete material properties ϵ_{xu} , v_u , and θ_u .

Yielding point

The shear force corresponding to the yielding of stirrups (V_y) is found from Eq. (2) of the original MCFT by assuming clamping stresses in the beam are negligible ($f_z = 0$),¹⁴ and multiplying the stress with the effective shear area

$$V_y = \frac{\rho_z f_{yt} + f_{c1y}}{\tan\theta_y} \cdot b d_v \quad (19)$$

f_{c1y} , which is the principal tensile stress in concrete when stirrups yield, is assumed to be equal to 20% of the concrete tensile strength ($0.2f'_t$). This assumption is made by incorporating the original formulation of the MCFT model and the post-cracking tension stiffening model of Tamai et al.²⁰ According to Eq. (5) of the original MCFT, the principal tensile strain in concrete at the yielding point (ϵ_{1y}) will be in the same order as the yielding strain of stirrups (ϵ_{2y}), considering that ϵ_{2y} is relatively larger than ϵ_{xy} and ϵ_{2y} at this stage of the response. Assuming that the typical yielding strain of stirrups (ϵ_{2y}) is approximately 0.002 and using the tension stiffening model of Tamai et al.,²⁰ f_{c1y} can be approximated as $0.2f'_t$. It is worth mentioning that because of the relatively gentle slope of the postpeak tensile response of concrete due to the tension stiffening effect, the influence of approximations made in determining f_{c1y} is insignificant.

To estimate θ_y in Eq. (19), the relationship between V and θ after the flexural cracking point (point 1) and before reaching the peak point (point 4) in the response is investigated for a wide range of RC beam sections using Response-2000. It is found that the relationship can be expressed in the form of

Eq. (20), where “ n ” is the shape factor, which can be varied from 0.5 to 1.0 in various beam sections. For simplicity, the shape factor at the yielding point is considered as 1.0, resulting in a linear relationship between V and θ . Equation (20) can be further simplified by approximating the shear force at the formation of flexural cracks (V_{fcr}) as 10% of the shear strength (V_u), and estimating the initial crack direction (θ_{fcr}) as 45 degrees, which is a reasonable assumption for RC sections. Applying these simplifications and rearranging Eq. (20) results in Eq. (21) for θ_y .

$$\left(\frac{\theta_{fcr} - \theta}{\theta_{fcr} - \theta_u}\right)^n + \left(\frac{V_u - V}{V_u - V_{fcr}}\right)^n = 1 \quad (20)$$

$$\theta_y = 45^\circ - (45^\circ - \theta_u) \left(\frac{1.11V_y}{V_u} - 0.11 \right) \quad (21)$$

By substituting θ_y from Eq. (21) into Eq. (19), the shear force at the yielding point (V_y) can be found as

$$V_y = \begin{cases} \frac{\left| \frac{k_{11}}{2k_{12}} \right|}{k_{12}} & k_{10}k_{12} > \left(\frac{k_{11}}{2}\right)^2, \theta_u \neq 45 \\ \frac{\frac{k_{11}}{2} - \sqrt{\left(\frac{k_{11}}{2}\right)^2 - k_{10}k_{12}}}{k_{10}} & k_{10}k_{12} \leq \left(\frac{k_{11}}{2}\right)^2, \theta_u \neq 45 \\ \frac{k_{11}}{k_{10}} & \theta_u = 45 \end{cases} \leq V_u \quad (22)$$

The calculation of shear strain at the yielding point is similar to that described for the peak shear strain and can be determined using Eq. (23)

$$\gamma_y = 2(\epsilon_{xy} + \epsilon_{2y}) \cdot \cot(\theta_y) \cdot k_{13} \leq \gamma_u \quad (23)$$

where ϵ_{xy} is estimated by calculating the average of longitudinal strains at the top and bottom of the section ($\epsilon_{xy.top}$ and $\epsilon_{xy.bot.}$), as shown in Eq. (24). $\epsilon_{xy.top}$ is approximately equal to the top longitudinal strain at the peak point ($\epsilon_{xu.top}$). Using this approximation, and ϵ_{xu} and X_u calculated in the previous section, $\epsilon_{xy.top}$ and $\epsilon_{xy.bot.}$ can be determined from Eq. (25) and (26), respectively

$$\epsilon_{xy} = \left| \frac{\epsilon_{xy.bot.} - \epsilon_{xy.top}}{2} \right| \leq \epsilon_{xu} \quad (24)$$

$$\epsilon_{xy.top} = \frac{k_1 V_u}{750} \cdot \frac{X_u}{d - X_u} \quad (25)$$

$$\epsilon_{xy.bot.} = \frac{k_1 V_y}{750} \quad (26)$$

The last parameter that needs to be determined in Eq. (23) is ϵ_{2y} . Using the results of the parametric study discussed previously, ϵ_{2y} is related to ϵ_{2u}

$$\epsilon_{2y} = \epsilon_{2u} \left(1 - \sqrt{1 - \frac{V_y}{V_u}} \right)^2 \quad (28)$$

where ϵ_{2u} can be calculated using Eq. (18). Finally, the parameter k_{13} in Eq. (23) is defined to account for the effective shear strain depth, as previously described for k_9 factor used for the ultimate point.

Flexural cracking point

The flexural cracking point is where the first crack perpendicular to the longitudinal axis of the beam develops. The flexural cracking moment is equal to $f'_t \times bh^2/6$. Therefore, the shear force corresponding to the cracking moment (V_{fcr}) can be determined according to Eq. (29).

$$V_{fcr} = \frac{0.33\sqrt{f'_c}bh^2}{6\alpha d_v} \quad (29)$$

The shear strain corresponding to the flexural cracking (γ_{fcr}) point is simply determined by dividing the shear force by the initial shear stiffness, as follows

$$\gamma_{fcr} = \frac{V_{fcr}}{Gb d_v} \quad (30)$$

Shear cracking point

After the section cracks, as the shear force increases, cracks start to rotate toward the concrete compression strut, forming diagonal shear cracks. According to the results of the parametric study, when the diagonal shear cracks reach approximately the middepth of the section, the neutral axis is located at the middepth of the section. In this study, this point is defined as the “shear cracking point” (refer to Fig. 1 and 3). Assuming a parabolic shear stress distribution through the section height, the average shear stress (v_{scr}) will be equal to two-thirds of the shear stress at the middepth of the section ($v_{scr.mid.}$)

$$v_{scr} = \frac{2}{3} v_{scr.mid.} \quad (31)$$

According to Eq. (3) of the original MCFT, $v_{scr.mid.}$ can be determined from the principal tensile and compressive stresses in concrete ($f_{c1.scr.mid.}$, $f_{c2.scr.mid.}$) and the crack inclination ($\theta_{scr.mid.}$) at the middepth of the section. Substituting Eq. (3) into Eq. (31) results in the following equation for the shear cracking force (V_{scr})

$$V_{scr} = \frac{2}{3} \frac{f_{c1.scr.mid.} + f_{c2.scr.mid.}}{\tan(\theta_{scr.mid.}) + \cot(\theta_{scr.mid.})} b d_v \quad (32)$$

where $f_{c1.scr.mid.}$ can be estimated as $f'_t = 0.33\sqrt{f'_c}$ (MPa) ($4\sqrt{f'_c}$ [psi]), because the shear cracking point is defined as when the concrete tensile stress at the middepth of the section reaches the cracking stress. $f_{c2.scr.mid.}$ is relatively small compared to $f_{c1.scr.mid.}$ at the shear cracking point.

Nevertheless, using the results of the parametric study, the following relationship between $f_{c2.scr.mid.}$, f'_c , and α can be found

$$f_{c2.scr.mid.} = \frac{7.7 f'_c}{(\alpha f'_c)^{1.6}} \quad (33)$$

If f'_c is expressed in imperial units, the 7.7 in Eq. (33) should be replaced by 22,000. $\theta_{scr.mid.}$ can also be found by calculating the average crack direction (θ_{scr}) and considering the distribution of the crack direction through the section height at the shear cracking point, as shown in Fig. 7. It can be seen that the distribution of crack direction can be approximated with a parabolic curve at the top half of the section and a constant value at the bottom half of the section. Using the weighted average concept, the crack direction at middepth can be estimated as approximately 1.5 times the average crack direction through the section

$$\theta_{scr.mid.} = 1.5\theta_{scr} \quad (34)$$

θ_{scr} is determined with the same concept as that provided for Eq. (20) at the yielding point, assuming that V_{scr}/V_u equals to 0.4 and 0.7 for beams with and without stirrups, respectively

$$\theta_{scr} = \begin{cases} 30^\circ + 0.33\theta_u & \text{with stirrups} \\ 15^\circ + 0.67\theta_u & \text{without stirrups} \end{cases} \quad (35)$$

The results of the sectional parametric study showed that the influence of the initial assumption for V_{scr}/V_u on the final value of V_{scr} is insignificant.

The shear cracking strain (γ_{scr}) is simply estimated by dividing the shear force by 75% of the initial shear stiffness of concrete, as presented in Eq. (36). The shear stiffness at this point can vary from Gbd_v to $0.5Gbd_v$. For simplicity, the average value of this range, $0.75Gbd_v$, is used for calculation.

$$\gamma_{scr} = \frac{V_{scr}}{0.75Gbd_v} \quad (36)$$

Failure point

For beams without stirrups or beams with stirrups that do not have adequate flexural reinforcement, the post-peak response is assumed to be negligible due to the brittle nature of the failure. For beams that contain stirrups and have adequate flexural reinforcement, a post-peak response is calculated to consider the residual shear strength and ductility of the beam after reaching the ultimate shear strength point. For these beams, the shear stress at failure is considered as 80% of the ultimate shear strength based on the recommendations from the literature.²¹ To find the shear strain, it is assumed that the principal compressive strain in concrete at failure (ϵ_{2f}) is equal to the strain corresponding to the peak compressive strength of concrete (ϵ_0). Using this assumption and Eq. (6) of the original MCFT, the shear strain at failure can be found from Eq. (37).

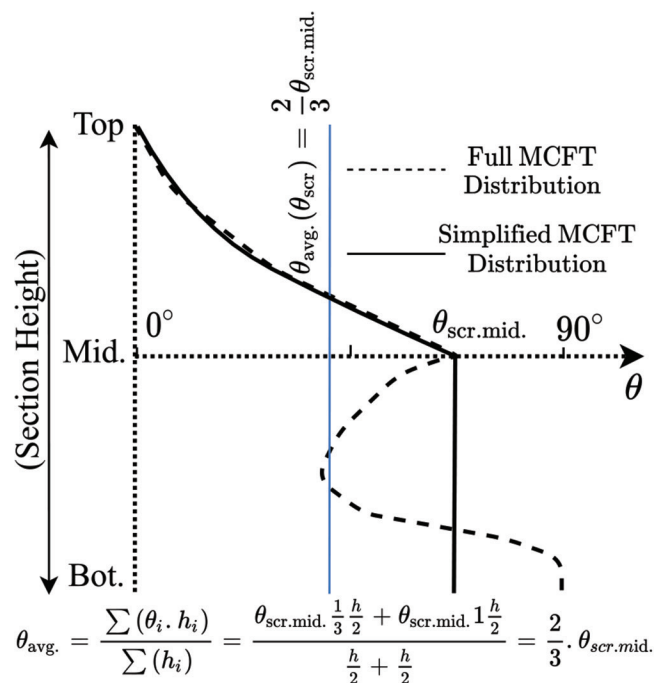


Fig. 7—Variation of crack direction through section at shear cracking point.

$$\gamma_f = 2(\epsilon_{xf} + \epsilon_0) \cot(\theta_f) k_{14} \quad (37)$$

Solving Eq. (37) requires estimating the average longitudinal strain (ϵ_{xf}) and the average crack direction (θ_f) at failure. It can be seen from various sectional analysis results that values of ϵ_x and θ at the postpeak response are approximately equal to those corresponding to the same shear force at the prepeak response. Thus, values of ϵ_x and θ at the failure point are approximated with the prepeak values at 80% of the shear strength. ϵ_{xf} can be found from the longitudinal strain at the top and bottom of the section ($\epsilon_{xf.bot.}$ and $\epsilon_{xf.top.}$) using Eq. (38)

$$\epsilon_{xf} = \left| \frac{\epsilon_{xf.bot.} - \epsilon_{xf.top.}}{2} \right| \geq \epsilon_{xu} \quad (38)$$

where $\epsilon_{xf.top.}$ is equal to $\epsilon_{xy.top.}$ as the top longitudinal strain does not vary significantly from the yielding point to the failure point and can be calculated using Eq. (25). Also, $\epsilon_{xf.bot.}$ can be calculated using Eq. (26) by replacing V_y with $0.8V_u$. The next parameter required to calculate the shear strain at failure is θ_f , which can be estimated by replacing V_y with $0.8V_u$ in Eq. (21). This results in the following simplified equation for θ_f .

$$\theta_f = 10^\circ + 0.78\theta_u \quad (39)$$

Finally, the parameter k_{14} is defined to account for the effective shear strain depth as previously described for k_9 and k_{13} factors used for the ultimate and yielding points, respectively.

The step-by-step procedure on how to use the aforementioned equations to calculate the five key points and generate the shear force-shear strain relationship is demonstrated in Fig. 8.

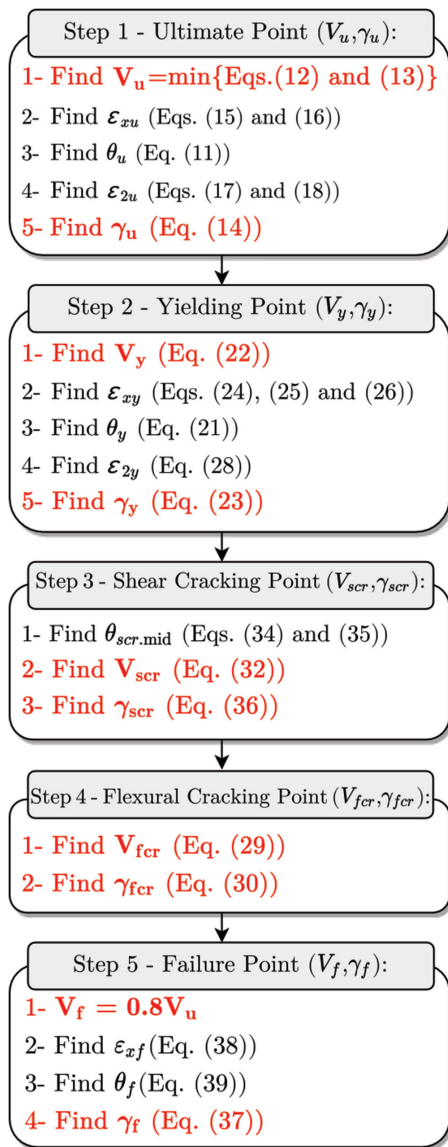


Fig. 8—Step-by-step procedure for calculation of five key points for proposed model.

VERIFICATION AT COMPONENT LEVEL

A total of 11 shear-critical beams experimentally tested by Podgorniak-Stanik,²² Frosch,²³ Cladera,²⁴ and Sherwood²⁵ and one flexural-critical beam tested by Kassem et al.²⁶ were selected to assess the performance and accuracy of the proposed model. To provide an unbiased comparison of the results, different beams were selected for the verification study than those considered in the previous section for the derivation of model equations. The main characteristics of the beams are shown in Table 1. The beam sections covered a wide range of key parameters to provide a comprehensive assessment of the proposed model. All beams were simply supported and subjected to a point load at the midspan, except for “ST-6” beam that was loaded under two symmetrical point loads.

The beams were modeled in the OpenSees²⁷ software using two-noded frame elements, each having a series of fibers representing the nonlinear behavior at the section level. As mentioned previously, the frame element in OpenSees is not capable of capturing the shear behavior in an RC member, because it is designed to consider only the biaxial flexure and axial behavior. To account for shear effects, the proposed shear hinge model was added to the FE model using *ZeroLength* elements (refer to Fig. 9). A *ZeroLength* element (that is, shear hinge) was placed on each side of the beam at d_v distance away from the applied load. This is considered to be the critical section for shear because the shear force distribution is constant throughout the beam and the largest bending moment occurs at the midspan under the loading plate. As the bending moment increases, the longitudinal strain increases, resulting in a lower shear strength and a more critical section (that is, shear force-bending moment interaction effect). Because of the high concentrated compressive force under the loading plate, the shear-critical section is typically assumed to be at the d_v distance away from the loading plate. This location correlates reasonably well with the location of diagonal shear cracks observed in experimental tests. It should be noted that this location is suitable only for simply

Table 1—Parameters of RC beams considered for verification study

Researcher	Beam	f'_c , MPa	f_{yt} , MPa	f_{ys} , MPa	b , mm	h , mm	d , mm	a , mm	s , mm	A_{st} , mm ²	A_{st} , mm ²	$V_{u,exp}/V_{u,cal}$
Kassem et al. ²⁶	ST-6	40.8	460	460	200	300	235	875	80	600	200	1.04
Podgorniak-Stanik ²²	BN50	37.0	483	—	300	500	450	1350	—	1100	—	1.14
	BH50	99.0	483	—	300	500	450	1350	—	1100	—	0.93
	BN100	37.0	550	—	300	1000	925	2700	—	2100	—	0.93
Sherwood ²⁵	S-10H	77.3	494	—	122	330	280	810	—	285	—	1.03
	L-10H	73.6	452	—	300	1510	1400	4050	—	3500	—	0.97
Podgorniak-Stanik ²²	BM100	46.0	550	508	300	1000	925	2700	600	2100	142.6	1.11
Frosch ²³	V1&V2	36.5	475	483	457	914	851	2553	372	3870	142.6	1.04
Sherwood ²⁵	S-10HS	77.3	502	496	122	330	280	810	160	458	19.6	1.13
	L-10HS	73.6	452	494	300	1510	1400	4050	235	5600	71.3	1.07
Cladera ²⁴	H50/4	49.9	500	540	200	400	351	1080	210	2098	100.6	1.04
	H100/4	87.0	500	540	200	400	351	1080	210	2098	100.6	0.99

Note: 1 mm = 0.0394 in.; 1 MPa = 0.145 ksi.

supported beams subjected to a concentrated load at the midspan. For beams with other types of boundary or loading conditions, the location of shear hinge might be different and should be selected based on the shear force and bending moment diagrams. A multilinear uniaxial material model was assigned to the *ZeroLength* elements. The response of the material model was defined using the values of the shear

force and shear deformation at each key point obtained from the procedure described in Fig. 8. The shear deformation was calculated by multiplying the shear strain by 1.5 times the section height (h), as recommended by Guner.²⁸

Figure 10 shows the comparison of load-deflection responses of the beams obtained from: 1) the experiment; 2) OpenSees with and without the proposed shear hinge model; 3) OpenSees with a shear hinge model defined according to the ASCE/SEI 41¹⁰ backbone curves; and 4) VecTor5,²⁹ a distributed plasticity analysis software with shear analysis capability. Before investigating the shear-critical beams, a flexural-critical beam (ST-6) was analyzed to verify the modeling procedure in OpenSees. It can be seen from Fig. 10 that the results of OpenSees models with and without the shear hinge for the flexural-critical beam were nearly identical and correlated well with the experimentally reported data. Thus, incorporating shear hinges into the OpenSees model did not have a noticeable effect on the behavior of the flexural-critical beam as expected. It is worth

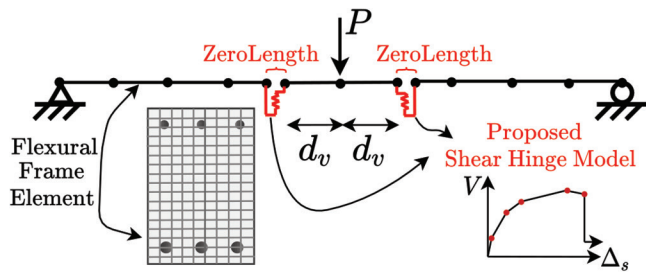


Fig. 9—OpenSees model of beam with proposed shear hinge model.

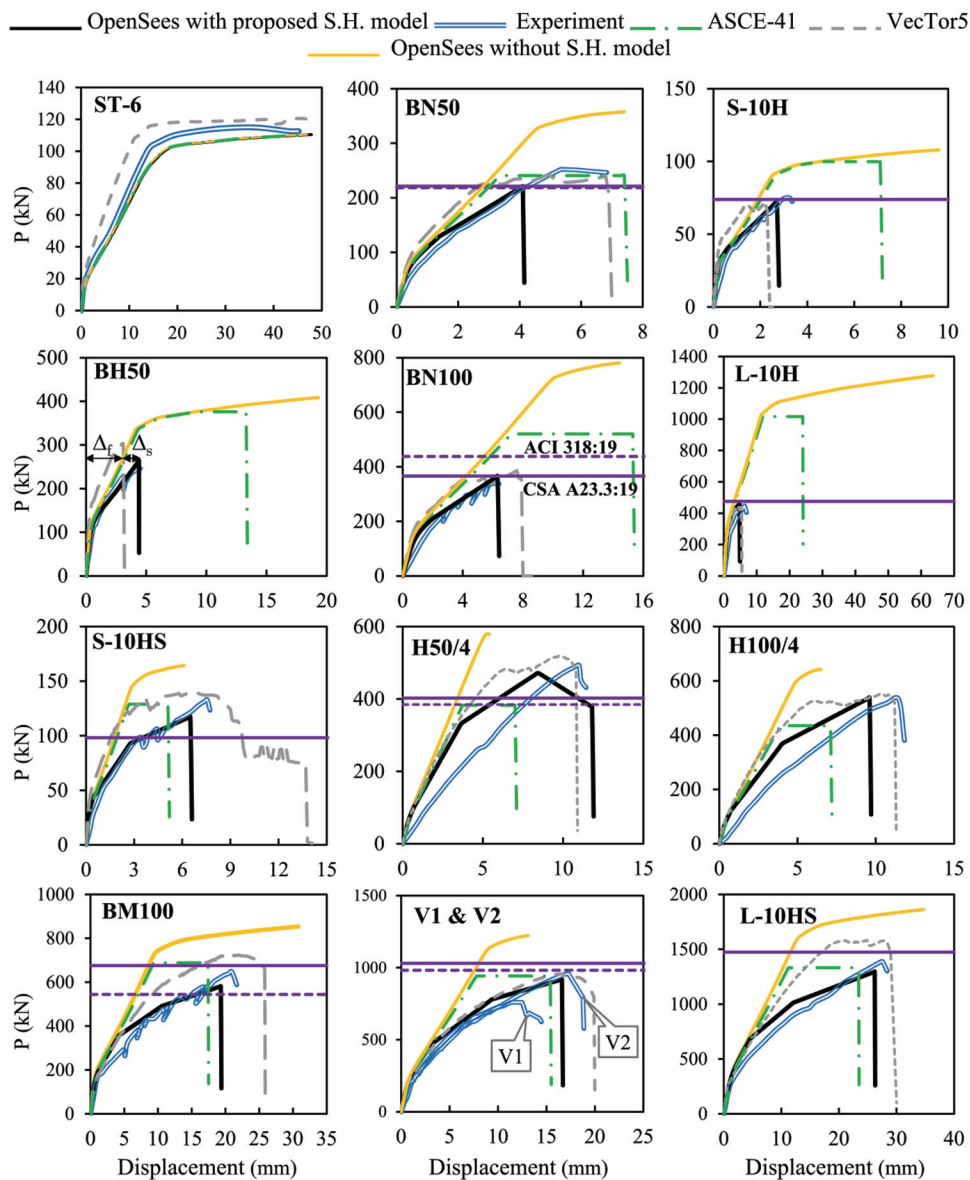


Fig. 10—Comparison of force-displacement curves between OpenSees models with and without proposed shear hinge, experiment, OpenSees with ASCE/SEI 41 shear hinge model, and VecTor5. (Note: 1 mm = 0.0394 in.; 1 kN = 0.225 kip.)

noting that for this beam the shear deformations were negligible compared with flexural deformations.

After verifying the FE modeling procedure in OpenSees, the ability of the proposed shear hinge model to capture shear behavior was investigated. It can be seen from Fig. 10 that the OpenSees model with the proposed shear hinge computed force-displacement relationships of the shear-critical beams reasonably well. In general, the model was able to capture the initial elastic response, reduction in stiffness caused by concrete cracking or yielding of the transverse reinforcement, peak strength and deformation, and failure due to shear. In some cases (H50/4 and H100/4), the model overestimated the initial stiffness, resulting in relatively more stiff responses with somewhat lower deflections. It is worth mentioning that the overestimation of the initial stiffness for these two beams was common for all analysis methods including the ASCE/SEI 41 shear hinge model and VecTor5. One reason for this could be that these beams might have already been in their cracked state prior to the test due to the shrinkage effect, which resulted in a lower initial stiffness compared with an uncracked beam. Another reason could be the inherent variation in the behavior of shear-critical test specimens due to the complexity and variability associated with shear mechanisms. An example of this variation can be seen in the experimentally reported peak strengths of V1 and V2 beams, which had identical material and structural characteristics.

As shown in Fig. 10, the OpenSees model without the shear hinge could not account for shear effects, leading to significant overestimation of the peak strength and deformation. For this model, the analysis continued until the beam reached its flexural capacity, resulting in wrong failure modes. It should be mentioned that frame elements with fiber sections in OpenSees are not intended to capture the shear behavior or to be used for analysis of shear-critical structures. The reason this modeling approach is included in this study is to demonstrate the consequence of using frame elements in OpenSees for structures with considerable shear effects and the importance of enhancing these elements with shear modeling capability.

Comparison of the load-deflection responses calculated by VecTor5, which considers shear effects using a distributed plasticity approach with those obtained from the proposed lumped plasticity shear hinge model in Fig. 10, demonstrated a good agreement between the results. Although the lumped plasticity model is based on a relatively less complicated analysis approach, where the nonlinearity effects resulting from shear are concentrated at the hinge locations, it can be seen that this approach resulted in the same or even higher level of accuracy compared with VecTor5. This can be due to an approximation made in the formulation of VecTor5, which assumes a predefined shear strain distribution (either parabolic or uniform) through the section for the entire analysis. This assumption, however, is only accurate for the initial stages of the response. After concrete starts to crack, shear strains at the cracked layers become considerably larger than those at the uncracked layers, resulting in a more complicated strain distribution. With the proposed shear hinge model, on the other hand,

the actual shear strain distribution in different stages of the response was considered in the derivation of the model equations in an average sense (refer to Fig. 3), which led to more accurate results for most of the analysis cases.

The performance of the proposed model was also evaluated against another shear hinge model defined based on the ASCE/SEI 41 backbone curves and implemented into OpenSees. It can be seen from Fig. 10 that this model could not accurately capture the strength and ductility of beams without stirrups, particularly if they had relatively high depth or high concrete compressive strength. One reason for this is the inability of the ASCE/SEI 41 model to consider the size effect, which is known to have a significant influence on the response of beams with little or no shear reinforcement.³⁰ For beams containing stirrups, the load-deflection responses calculated by the ASCE-41 model generally showed better agreement with the experimental results.

The shear strength of the beam sections predicted by the CSA A23.3¹³ and ACI 318-19³¹ design codes are also shown in Fig. 10. ACI 318 and CSA A23.3 equations are not applicable to beams that have f'_c of greater than 70 and 80 MPa (10.15 and 11.60 ksi), respectively. Therefore, the results related to these beams are not presented. The peak strength calculated by the proposed shear hinge model and CSA A23.3 for beams without stirrups were close to each other and showed better agreement with the experimental results when compared with the peak strength obtained from ACI 318. For beams with stirrups, the proposed shear hinge model computed the peak strength of beams more accurately than both of the design codes.

VERIFICATION AT SYSTEM LEVEL

The application of the proposed model at the system level was investigated on a two-story, single-span RC frame with shear-critical beams tested by Duong et al.³² The geometry

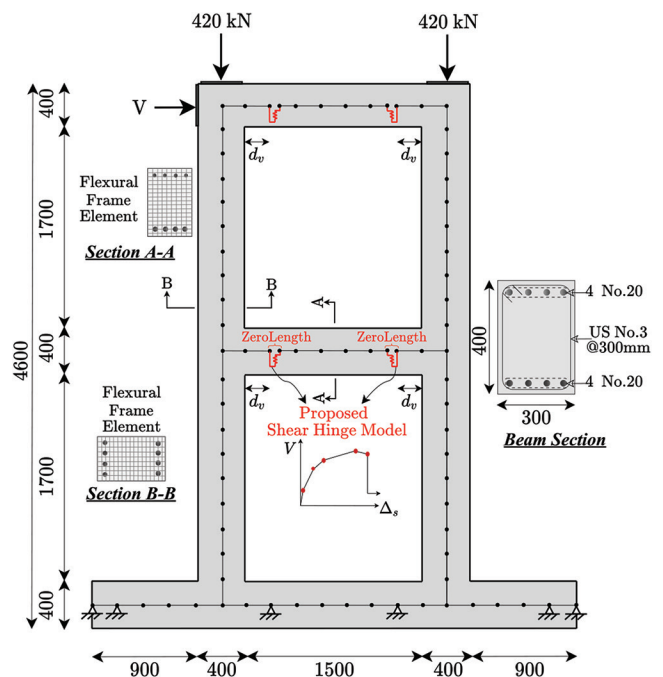


Fig. 11—Duong et al.³² test frame. (Note: 1 mm = 0.0394 in.; 1 kN = 0.225 kip.)

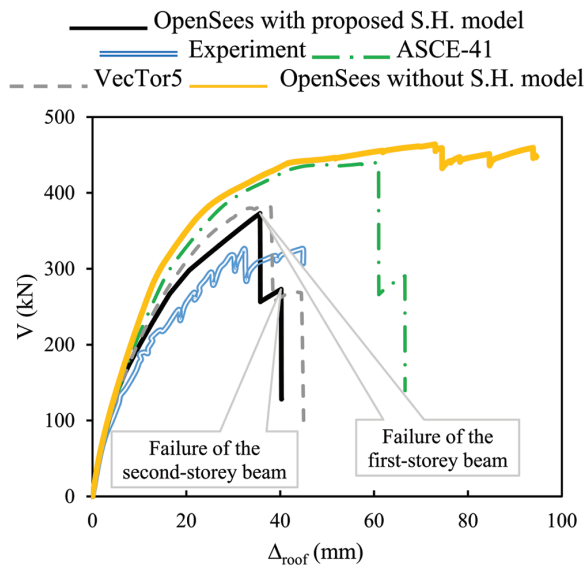


Fig. 12—Comparison of base shear versus lateral roof displacement for Duong et al.³² test frame. (Note: 1 mm = 0.0394 in.; 1 kN = 0.225 kip.)

of the frame, as well as cross-section dimensions and reinforcement details, are shown in Fig. 11. The base shear versus lateral roof displacement responses reported from the experimental test and calculated by the analysis procedures mentioned in the previous section are shown in Fig. 12. It can be seen that there was good agreement between the results of the OpenSees model with the proposed shear hinge model, the VecTor5 model, and the experiment. Both analytical models captured the damage sequence and failure mode of the frame accurately. First, the first-storey beam failed in shear, causing a significant drop in the load-deflection response, which was shortly followed by the shear failure of the second-storey beam, resulting in complete failure of the frame. The other two analytical models (OpenSees model without shear hinge and OpenSees model with ASCE/SEI 41 shear hinge) both significantly overestimated the peak strength and ductility. The OpenSees model without shear hinge only computed the flexural response of the frame and neglected the shear behavior, as expected. The OpenSees model with the ASCE/SEI 41 shear hinge captured the shear failure but significantly overestimated the peak shear strength and ductility of the frame. One reason for the overestimation of the results is that the ASCE/SEI 41 model does not take into account the influence of yielding of longitudinal reinforcement on the shear capacity, as discussed in the derivation of the ultimate strength equation in the Model Development section. The overestimation in the strength led to significantly higher lateral roof deformations, especially because at this stage of the response, the flexural reinforcement at the base of the columns had yielded.

SUMMARY AND CONCLUSIONS

A nonlinear lumped plasticity model was developed based on the Modified Compression Field Theory (MCFT) to capture the shear behavior of reinforced concrete (RC) beams. The compatibility, equilibrium, and constitutive relationships of the original MCFT model, which requires a complicated

trial-and-error procedure, were simplified into closed-form equations using a wide range of parametric studies on shear-critical RC beams. Nonlinear distribution of stresses, strains, and crack direction through the section at different stages of the response was considered in the development of the model equations. Using the proposed model, the shear force and shear deformation values at five key stages of the response can be calculated, enabling detailed representation of the shear behavior. By implementing the proposed model into OpenSees, its performance was assessed against experimental tests, the ASCE/SEI 41 lumped plasticity model, and a distributed plasticity model at both the component and system level. It was demonstrated that the proposed model can compute the failure mode and load-deflection response of the test specimens with better accuracy compared with the other two modeling approaches. The analysis results also highlighted the consequences of using a frame-type analysis procedure such as OpenSees for shear-critical structures without giving special consideration to modeling shear effects. Lastly, the ultimate shear strength values estimated from the proposed model were compared against those obtained from the CSA A23.3 and ACI 318 design codes. It was shown that although the basis of the proposed model is similar to CSA A23.3 for the calculation of the ultimate shear strength, the model provided more accurate results because of the improvements made in the formulation.

After successful application of MCFT to various design procedures and nonlinear FE and sectional analysis programs over the last 35 years, this study for the first time demonstrated that this viable theory can also be highly effective for the analysis of shear-critical RC structures using the lumped plasticity approach. Considering the computational efficiency of the lumped plasticity approach, the proposed shear hinge model will be beneficial for the analysis of large RC structural systems. It enables the nonlinear shear response of structures to be accurately taken into account while using computationally efficient frame-type analysis procedures.

AUTHOR BIOS

Amir Reza Tabkhi Wayghan is an MSc Student at Carleton University, Ottawa, ON, Canada. He received his BSc and MSc in civil engineering and structural engineering, respectively, from the Sharif University of Technology, Tehran, Iran. His research interests include assessment of reinforced concrete structures, fiber-reinforced polymer sheets, reinforcing bar applications, and performance-based design.

Vahid Sadeghian is an Assistant Professor in the Department of Civil and Environmental Engineering at Carleton University. His research interests include nonlinear analysis and design of concrete structures, constitutive modeling, performance assessment and forensic investigation, and repair and rehabilitation of structures.

NOTATION

A_{sl}	=	area of tensile longitudinal reinforcement
A_{st}	=	area of transverse reinforcement
a	=	shear span
b	=	beam width
d	=	effective depth
d_v	=	effective shear depth, taken as the greater of $0.9d$ or $0.72h$
E_s	=	modulus of elasticity of steel
f'_c	=	cylindrical compressive strength of concrete
f_{c1}	=	principal tensile stress in concrete
f_{c2}	=	principal compressive stress in concrete
f_{sx}	=	average stress in x -reinforcement
f_{sz}	=	average stress in z -reinforcement

f'_t	=	modulus of rupture of concrete
f_x	=	stress applied to element in x -direction
f_{yt} (f_{yx})	=	yield strength of longitudinal reinforcement
f_{yt} (f_{yz})	=	yield strength of transverse reinforcement
f_z	=	stress applied to element in z -direction
G	=	initial shear modulus of concrete
h	=	beam height
n	=	shape factor used in Eq. (20)
s	=	spacing of transverse reinforcement
s_z	=	crack spacing parameter, as defined in CSA A23.3
s_{ze}	=	equivalent value of s_z that allows for influence of aggregate size
V	=	shear force
V_c	=	shear resistance provided by concrete
V_f	=	shear force acting on a section
V_r	=	shear resistance
V_s	=	shear resistance provided by transverse reinforcement
v	=	shear stress
v_c	=	shear stress in concrete
v_{ci}	=	shear stress on crack surfaces
X	=	distance from extreme compression fiber to neutral axis
α	=	M/Vd_v
β	=	contribution factor accounting for strength of cracked concrete
Δ_f	=	flexural deformation
Δ_s	=	shear deformation
ϵ_0	=	strain in concrete at peak stress f'_c
ϵ_1	=	principal tensile strain in concrete
ϵ_2	=	principal compressive strain in concrete
ϵ_x	=	longitudinal strain
ϵ_z	=	transverse strain
γ	=	shear strain
θ	=	angle between crack inclination and x -axis
ρ_x	=	longitudinal reinforcement ratio
ρ_z	=	transverse reinforcement ratio

Subscripts u , f , y , scr , and fer are related to each of the five key points in the model. Also, subscripts $mid.$, top , and bot . show the location of the parameter through the height of the section. Parameters without the location subscripts indicate the average value through the height. For example, θ_y denotes the average crack inclination angle at the yielding point, and $f_{c1,scr,mid}$ denotes the principal tensile stress in concrete at the middepth of the section at the shear cracking point.

REFERENCES

- Selby, R. G.; Vecchio, F. J.; and Collins, M. P., "The Failure of an Offshore Platform," *Concrete International*, V. 19, No. 8, Aug. 1997, pp. 28-35.
- Johnson, P. M., and Commission d'enquête sur le viaduc de la Concorde Québec, "Report of the Commission of Inquiry into the Collapse of a Portion of the de la Concorde Overpass," Commission d'enquête sur le viaduc de la Concorde Québec, Gouvernement du Québec, Québec, QC, Canada, 2007, 222 pp.
- Bouchaboub, M., and Samai, M. L., "Nonlinear Analysis of Slender High-Strength R/C Columns under Combined Biaxial Bending and Axial Compression," *Engineering Structures*, V. 48, Mar, 2013, pp. 37-42. doi: 10.1016/j.engstruct.2012.08.030
- Simão, P. D.; Barros, H.; Ferreira, C. C.; and Marques, T., "Closed-Form Moment-Curvature Relations for Reinforced Concrete Cross Sections under Bending Moment and Axial Force," *Engineering Structures*, V. 129, Mar. 2016, pp. 67-80. doi: 10.1016/j.engstruct.2016.09.033
- Pincheira, J. A.; Dotiwala, F. S.; and D'Souza, J. T., "Seismic Analysis of Older Reinforced Concrete Columns," *Earthquake Spectra*, V. 15, No. 2, 1999, pp. 245-272. doi: 10.1193/1.1586040
- Shirai, N.; Moriizumi, K.; and Terasawa, K., "Cyclic Analysis of RC Columns: Macro-Element Approach," *Proceedings, Modeling of Inelastic Behavior of RC Structures under Seismic Loads*, American Society of Civil Engineers, Reston, VA, 2001, pp. 435-453.
- Elwood, K. J., "Modelling Failures in Existing Reinforced Concrete Columns," *Canadian Journal of Civil Engineering*, V. 31, No. 5, 2004, pp. 846-859. doi: 10.1139/104-040
- LeBorgne, M. R., and Ghannoum, W. M., "Analytical Element for Simulating Lateral-Strength Degradation in Reinforced Concrete Columns and Other Frame Members," *Journal of Structural Engineering*, ASCE, V. 140, No. 7, 2014, p. 04014038. doi: 10.1061/(ASCE)ST.1943-541X.0000925
- Sae-Long, W.; Limkatanyu, S.; Prachasaree, W.; Horpibulsuk, S.; and Panedpojaman, P., "Nonlinear Frame Element with Shear-Flexure Interaction for Seismic Analysis of Non-Ductile Reinforced Concrete Columns," *International Journal of Concrete Structures and Materials*, V. 13, No. 1, 2019, pp. 1-19. doi: 10.1186/s40069-019-0343-2
- ASCE/SEI 41-17, "Seismic Evaluation and Retrofit of Existing Buildings," American Society of Civil Engineers, Reston, VA, 2017, 576 pp.
- Vecchio, F. J., and Collins, M. P., "The Modified Compression-Field Theory for Reinforced Concrete Elements Subjected to Shear," *ACI Journal Proceedings*, V. 83, No. 22, Mar.-Apr. 1986, pp. 219-231.
- Sadeghian, V., and Vecchio, F., "The Modified Compression Field Theory: Then and Now," *Shear in Structural Concrete*, SP-328, American Concrete Institute, Farmington Hills, MI, Sept. 2018, pp. 3.1-3.20.
- CSA A23.3, "Design of Concrete Structures," Canadian Standards Association, Mississauga, ON, Canada, 2019, 296 pp.
- Bentz, E. C.; Vecchio, F. J.; and Collins, M. P., "Simplified Modified Compression Field Theory for Calculating Shear Strength of Reinforced Concrete Elements," *ACI Structural Journal*, V. 103, No. 4, July-Aug. 2006, pp. 614-624.
- Esfandiari, A., and Adebar, P., "Shear Strength Evaluation of Concrete Bridge Girders," *ACI Structural Journal*, V. 106, No. 4, July-Aug. 2009, pp. 416-426.
- Bentz, E., and Collins, M. P., 2001, "Response-2000, Shell-2000, Triax-2000, and Membrane-2000 User Manual (Version 1.0 and 1.1)," Sept. 2001, <http://www.ecf.utoronto.ca/~bentz/manual2/final.pdf>.
- Bentz, E. C., and Collins, M. P., "Development of the 2004 Canadian Standards Association (CSA) A23.3 Shear Provisions for Reinforced Concrete," *Canadian Journal of Civil Engineering*, V. 33, No. 5, 2006, pp. 521-534. doi: 10.1139/106-005
- Park, R., and Paulay, T., *Reinforced Concrete Structures*, John Wiley & Sons, Inc., New York, 1975, 769 pp.
- Hognestad, E., "Study of Combined Bending and Axial Load in Reinforced Concrete Members," University of Illinois Engineering Experiment Station, Bulletin No. 399, V. 49, No. 22, 1951, 128 pp.
- Tamai, S.; Shima, H.; Izumo, J.; and Okamura, H., "Average Stress-Strain Relationship in Post Yield Range of Steel Bar in Concrete," *Concrete Library of JSCE*, No. 11, June 1988, pp. 117-129.
- Park, Y., and Ang, A., "Mechanistic Seismic Damage Model for Reinforced Concrete," *Journal of Structural Engineering*, ASCE, V. 111, No. 4, 1985, pp. 722-739. doi: 10.1061/(ASCE)0733-9445(1985)111:4(722)
- Podgorniak-Stanik, B. A., "The Influence of Concrete Strength, Distribution of Longitudinal Reinforcement, Amount of Transverse Reinforcement and Member Size on Shear Strength of Reinforced Concrete Members," MASC thesis, University of Toronto, ON, Canada, 1998, 369 pp.
- Frosch, R. J., "Behavior of Large-Scale Reinforced Concrete Beams with Minimum Shear Reinforcement," *ACI Structural Journal*, V. 97, No. 6, Nov.-Dec. 2000, pp. 814-820.
- Cladera, A., "Shear Design of Reinforced High-Strength Concrete Beams," PhD thesis, Universitat Politècnica De Catalunya, Barcelona, Spain, 2002, 325 pp.
- Sherwood, E., "One-Way Shear Behaviour of Large, Lightly-Reinforced Concrete Beams and Slabs," PhD thesis, University of Toronto, Toronto, ON, Canada, 2008, 567 pp.
- Kassem, C.; Farghaly, A. S.; and Benmokrane, B., "Evaluation of Flexural Behavior and Serviceability Performance of Concrete Beams Reinforced with FRP Bars," *Journal of Composites for Construction*, ASCE, V. 15, No. 5, 2011, pp. 682-695. doi: 10.1061/(ASCE)CC.1943-5614.0000216
- Mazzoni, S.; McKenna, F.; Scott, M. H.; and Fenves, G. L., "OpenSees Command Language Manual," Pacific Earthquake Engineering Research (PEER) Center, University of California, Berkeley, Berkeley, CA, 2006.
- Guner, S., "Performance Assessment of Shear-Critical Reinforced Concrete Plane Frames," PhD thesis, University of Toronto, Toronto, ON, Canada, 2008, 429 pp.
- Guner, S., and Vecchio, F. J., 2008, "User's Manual of VecTor5," <http://www.vectoranalysisgroup.com/software.html>. (last accessed Sept. 15, 2021).
- Collins, M. P.; Quach, P. T.; and Bentz, E. C., "Shear Behavior of Thick Slabs," *ACI Structural Journal*, V. 117, No. 4, July 2020, pp. 115-126.
- ACI Committee 318, "Building Code Requirements for Structural Concrete (ACI 318-19) and Commentary (ACI 318R-19)," American Concrete Institute, Farmington Hills, MI, 2019, 624 pp.
- Duong, K. V.; Sheikh, S. A.; and Vecchio, F. J., "Seismic Behavior of Shear-Critical Reinforced Concrete Frame: Experimental Investigation," *ACI Structural Journal*, V. 104, No. 3, May-June 2007, pp. 304-313.

Appendix—Equations for factors

$k_1 = \frac{750(1+\alpha)}{A_s E_s}$	$k_2 = 0.4\sqrt{f'_c}bd_v \frac{1300}{1000+s_{ze}} \text{ (SI)}$ $\left(k_2 = 4.8\sqrt{f'_c}bd_v \frac{51}{39+s_{ze}} \text{ (Imperial)} \right)$		$k_3 = 1.73\xi$	$k_4 = 1 + 0.2\xi k_1$
$k_5 = \frac{\frac{h}{2} - X_u}{d - X_u}$	$k_6 = \begin{cases} 1.0 & \frac{\rho_z f_{yt}}{f'_c} \geq 0.1 \\ \left(\frac{\rho_z f_{yt}}{0.1 f'_c} \right)^{0.2} & 0 < \frac{\rho_z f_{yt}}{f'_c} < 0.1 \\ 0.88 + \frac{s_{ze}}{2500} \leq 1.3 \text{ (SI)} \left(0.88 + \frac{s_{ze}}{98} \leq 1.3 \text{ (Imperial)} \right) & \frac{\rho_z f_{yt}}{f'_c} = 0 \text{ (without stirrups)} \end{cases}$			
$k_7 = 440 - \frac{206}{\left[1 + \left(\frac{s_{ze}}{450} \right)^5 \right]^{18}} \text{ (SI)}$ $\left(k_7 = 440 - \frac{206}{\left[1 + \left(\frac{s_{ze}}{17.7} \right)^5 \right]^{18}} \text{ (Imperial)} \right)$		$k_9 = \frac{h}{d - X_u}$		
$k_{10} = (\rho_z f_{yt} + f_{c1y})bd_v$		$k_8 = \mu \epsilon_0 - 1 + \sqrt{(\mu \epsilon_0 - 1)^2 + 4\mu \epsilon_{sv} \frac{\delta}{\delta + 1} + 0.8 \frac{f_{c2u}}{f'_c}}$		
$k_{11} = \frac{400 - \theta_u}{360}$	$k_{12} = \frac{45 - \theta_u}{36V_u}$	$k_{13} = \frac{h}{d - X_y}$	$k_{14} = \frac{h}{d - X_p}$	
$k_{15} = \frac{A_{st} f_{yt} d_v}{s}$	$\alpha = \frac{M_f}{V_f d_v} \geq 1.0$	$\delta = \sqrt{1 + \tan^2(2\theta_u)}$	$\xi = \frac{A_{st} f_{yt} d_v}{\left(\frac{\rho_z f_{yt}}{0.1 f'_c} \right)^{0.23} s}$	$\mu = 85 \frac{\delta + 1}{\delta - 1} \frac{f_{c2u}}{f'_c}$
$X_y = \frac{\epsilon_{xy,top}}{\epsilon_{xy,top} + \epsilon_{xy,bot}} d$	$X_p = \frac{\epsilon_{xp,top}}{\epsilon_{xp,top} + \epsilon_{xp,bot}} d$		$s_{ze} = \begin{cases} \frac{35s_z}{15 + a_g} \geq 0.85s_z & \text{with stirrups (SI)} \\ 300 \text{ mm} & \text{without stirrups} \end{cases}$ $\left(s_{ze} = \begin{cases} \frac{1.38s_z}{0.59 + a_g} \geq 0.85s_z & \text{with stirrups (Imperial)} \\ 11.81 \text{ in.} & \text{without stirrups} \end{cases} \right)$	

ACI Faculty Network

Why Join the Faculty Network

The Faculty Network is a support group for educators interested in ACI and the concrete industry. Members receive notifications about classroom resources, fellowships and scholarships, funding for research, online learning, and calls for papers and presenters.

Free 1-Year Educator Membership

ACI offers complimentary membership to teaching professionals who have not been an ACI member within the past 5 years.


Free Desk Copies

Faculty Network members can request a complimentary print or pdf copy of:


- ACI 318-19, Building Code Requirements for Structural Concrete
- SP-4, Formwork for Concrete
- ACI 530, Building Code Requirements and Specification for Masonry Structures and Companion Commentaries
- MNL-17, The ACI Reinforced Concrete Design Handbook
- MNL-5(19): Contractor's Guide to Quality Concrete Construction, 4th Edition
- ACI 562-19, Code Requirements for Assessment, Repair, and Rehabilitation of Existing Concrete Structures

Networking

ACI hosts a Faculty Network Reception twice a year during the ACI Concrete Conventions, giving an opportunity to exchange ideas and network.

 Faculty Network members receive a complimentary annual subscription that provides users with convenient digital interactive access to ACI CODE-318-19, along with in-document access to related resources and enhanced digital search features through all code provisions and commentary. The platform allows professors and students to view and share digital notes and the additional resources within the platform.



 Professors' Workshop

CO-SPONSORED BY PCA EDUCATION FOUNDATION AND ACI FOUNDATION
Materials | Pavements | Structures

The Professors' Workshop is designed to provide instructors in civil engineering, architecture, architectural engineering, materials science, and construction management programs the tools to engage students in the latest developments in concrete design, construction, and materials.



The Concrete Research Council (CRC) seeks concrete research projects that further the knowledge and sustainability of concrete materials, construction, and structures in coordination with ACI Committees. Annual Request for Proposals (RFP) are received between August 1 and December 1.



American Concrete Institute
Always advancing

Join online at www.concrete.org/educatorsandresearchers/facultynetwork